INDERSCIENCE PUBLISHERS
Linking academia, business and industry through research

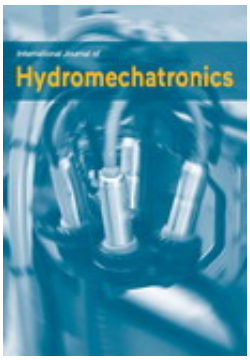

International Journal of Hydromechatronics

ISSN online: 2515-0472 - ISSN print: 2515-0464
https://www.inderscience.com/ijhm

Development of a torque motor with enhanced performance employing novel semi-inset PM pole

Xinghua He, Pengjie Xiang, Zhihao Xu, Xiaocheng Wei, Yue Li

DOI: 10.1504/IJHM.2025.10069814

Article History:

Received:	11 May 2024
Last revised:	06 November 2024
Accepted:	10 December 2024
Published online:	14 March 2025

Copyright © 2025 Inderscience Enterprises Ltd.

Development of a torque motor with enhanced performance employing novel semi-inset PM pole

Xinghua He, Pengjie Xiang* and Zhihao Xu

School of Automation Science and Electrical Engineering,
Beihang University,
Beijing 100191, China
and
Tianmushan Laboratory,
Xixi Octagon City, Yuhang District,
Hangzhou 310023, China
and
Science and Technology on Aircraft Control Laboratory,
Beihang University,
Beijing 100191, China
Email: by2003105@buaa.edu.cn
Email: xiangpengjie@163.com
Email: xuzhihao@buaa.edu.cn
*Corresponding author

Xiaocheng Wei

Ningbo Institute of Technology,
Beihang University,
Ningbo 315800, China
Email: xiaocheng_wei@163.com

Yue Li

School of Automation Science and Electrical Engineering,
Beihang University,
Beijing 100191, China
Email: liyuebh@163.com

Abstract: The key task of torque motors is to enhance the output torque. From an electromagnetic design perspective, the motor is required to have the largest possible air gap flux density and operating current. This can be achieved through several approaches: First, by using high-performance permanent magnets to increase the rotor magnetic flux. Second, by employing high-permeability soft magnetic materials to reduce magnetic reluctance. Third, through more rational structural design. Fourth, by designing efficient heat dissipation structures. Based on these approaches, a torque motor with enhanced performance employing novel semi-inset PM pole is proposed, the structure of the motor is introduced, the influence of the new semi-inset permanent magnet poles on the electromagnetic performance is analysed, the

Copyright © The Author(s) 2025. Published by Inderscience Publishers Ltd. This is an Open Access Article distributed under the CC BY-NC-ND license. (http://creativecommons.org/licenses/by-nc-nd/4.0/)

structural strength and temperature rise are checked, and finally a prototype is manufactured and its performance is verified. The design results have achieved the expected effect and meet the given operating conditions.

Keywords: torque; magnetic pole pattern; electromagnetic field; permanent magnet machine; finite element simulation.

Reference to this paper should be made as follows: He, X., Xiang, P., Xu, Z., Wei, X. and Li, Y. (2025) 'Development of a torque motor with enhanced performance employing novel semi-inset PM pole', *Int. J. Hydromechatronics*, Vol. 8, No. 5, pp.40–54.

Biographical notes: Xinghua He received his BS and MS degrees in Engineering from Liaoning Technical University, Fuxin, China, in 2014 and 2017, respectively. He is currently working towards his PhD degree in Mechatronics from Beihang University, Beijing, China. His research interests include electromagnetic actuators and permanent magnet machines.

Pengjie Xiang received his BS degree in Engineering from Lanzhou University of Technology, Lanzhou, China, in 2020. He is currently working towards his PhD degree in Mechatronics from Beihang University, Beijing, China. His research interests include the design and control of permanent magnet machines.

Zhihao Xu received his BS degree in Engineering from the Jilin University, Changchun, China, in 2022. He is currently working towards his MS degree in Mechatronics from Beihang University, Beijing, China. His research interests include permanent magnet machines and electromagnetic actuators.

Xiaocheng Wei received his Bachelor and Master degree from North University of China, Taiyuan, China, in 2014 and 2017, respectively. In 2022, he received his PhD degree in Electrical Machines from University of Nottingham, UK. He is currently with Ningbo Institute of Technology, Beihang University, Ningbo, China, as an Associate Professor. His research interests include high-performance motor, hybrid electric propulsion system and PM generator.

Yue Li received her BS degree in Engineering from Northeast Agricultural University, Harbin, China, in 2020. She received her MS degree in Mechatronics from Beihang University, Beijing, China, in 2023. Her research interests include permanent magnet machines and electromagnetic actuators.

1 Introduction

Compared to traditional driving systems with gearbox, direct drive torque motor makes the system more concise and reliable (Liu et al., 2007; Yu et al., 2023; Zhang et al., 2023). Torque motors are widely used in hydraulic pumps (Ding et al., 2024; Panwar and Michael, 2018; Qiu et al., 2022). Since such kinds of motors often have low speeds and high torque requirements, enhancing the output torque of torque motors is a key research focus (Yu et al., 2023; Zhang et al., 2023). As the mechanism of motor torque generation involves the interaction between the rotor magnetic field and the stator magnetic field, enhancing the magnitude of both is crucial for increasing motor output torque (Pyrhonen

et al., 2013). For the rotor, the strength of the magnetic field intensity can be enhanced using high-performance permanent magnets, whereas for the stator, a higher current is necessary to generate a greater magneto-motive force. In addition, minimising the magnetic resistance of the magnetic circuit is necessary to achieve a higher air gap magnetic density, thereby achieving stronger energy conversion. However, increasing the current will inevitably increase the Joule heating of the winding, leading to excessive temperatures. Therefore, achieving an increase in torque requires not only reasonable thermal scheme but also better electromagnetic design.

There are three types of PM rotors, i.e., interior, inset, and surface-mounted pole. Among them, interior motors are widely used in vehicle motors due to its wide range of speed under control (Liu et al., 2016, 2015; Yamazaki et al., 2022), especially the V-type interior PM motor which has been employed from Toyota Prius 2004 to Prius 2010 (Burress et al., 2011; Hsu, 2004). However, since this type of motor has a large rotor mass and a complex design process, its application in the field of low-speed motors and micro motors is rare.

In order to achieving high torque density, the rotor type of torque motors often employs surface-mounted pole (Yan et al., 2019, 2008, 2006). Building on the concept of traditional radial alternating magnetic poles, Zheng et al. (2007) adopts an eccentric magnetic pole to decrease the torque ripple. To avoid reducing output torque too much while decrease the torque ripple, harmonic compensated pole is proposed to optimise the performance of surface-mounted PMSM by Zeng et al. (2020). Related studies consist of sinusoidal arc shaping using third-order harmonics and inverse cosine shaping with third-order harmonics conducted by Shen and Zhu, (2012). There are also some methods that have similar effects and purposes to harmonic compensation although their principles are different. For example, Isfahani et al. (2008) splices high-quality PM and low-quality PM together, with high-quality PM in the middle of the magnetic pole and low-quality PM at both ends, and Ashabani and Mohamed (2011) divides the permanent magnet into three sections along the tangential direction, with the middle section wide and the two end sections narrow. In addition, many special shaped magnetic poles is proposed such as bread shaped (Jang et al., 2011), semi-circular shaped (Xiang et al., 2023), combination of triangles and rectangles (Dong et al., 2023).

However, due to the fact that the PMs often glued directly on the surface of rotor, there is always a risk of detachment, especially when using the Halbach array as the rotor magnetic pole. Therefore, many motor designs require carbon fibre or stainless-steel sleeves to be wrapped around the rotor. For example, the rotor of the propulsion motor on NASA's X57 all-electric aircraft (Hall et al., 2019) is wrapped by carbon fibre with the thick of 0.381 mm. This design inevitably increases the electromagnetic air gap, which compromise torque enhancement.

Therefore, this paper proposes a torque motor with enhanced performance employing novel semi-inset PM pole which simultaneously improve output characteristics and rotor structural strength, a heat dissipation structure based on actual operating environment. The content of this article is arranged as follows: In the Section 2, the overall structure of a motor is determined for a specific design requirement and the work principle of the proposed structure are introduced. In the Section 3, electromagnetic simulations of the pole configuration are conducted, studying the impact of different structural parameters on air-gap flux density. The structural strength and temperature rise of the electromagnetic structure are verified in the Section 4. Finally, prototypes are fabricated and experimentally validated.

2 Overall structure and work principle

2.1 Design requirements and overall structure

To elaborate the proposed method clearly, a specific motor is designed for an aviation air compressor pump with the design requirements shown in Table 1. Based on the design requirements outlined above, the overall structure of the motor has been designed as illustrated in Figure 1. The motor primarily comprises a stator, rotor, housing, front and rear end covers. A resolver is installed at the rear of the motor to determine the relative positions between the rotor and stator. A pedestal is situated at the bottom to accommodate horizontal installation requirements. Given that natural convection flows perpendicular to the motor axis, the housing features annular fins. The motor adopts a configuration of 12 slots and 10 poles. Unlike conventional rotors, the rotor core of the motor features a small protrusion, forming a T-shaped slot where the rotor magnetic pole with a notch is embedded, thereby reducing the risk of magnetic pole detachment.

Table 1 The design specifications and requirements for the air compressor motor

Item	*Value*	*Unit*
Rated power	320	W
Rated speed	800	r/min
Mass	≤ 3	kg
Length	≤ 110	mm
Diameter	≤ 110	mm
Ambient temperature	–55～70	℃
Power supply (DC)	270	V
Cooling mode	Natural convection	-
Mounting type	Foot	-

Table 2 The materials assigned to each component

Component	*Material*	*Component*	*Material*
Stator lamination	1J22	Housing	7,075
Rotor core	20Cr13	Permanent magnet	N35EH

Due to the protrusion of the rotor core not playing a decisive role in the motor's output torque and merely potentially improving certain performance aspects, the primary structural parameters do not account for this component. The rotor structure is considered to be a common tile-shaped surface-mounted magnet, and the materials of each component are listed in Table 2. The rotor is made of solid magnetic material, since it is easy to manufacture and has a high structural strength. The structural dimensions of the rotor can be obtained by some optimisation method such as the multi-objective optimisation method for surface-mounted PMSM with fixed torque output (He et al., 2023) as shown in Table 3. Subsequently, based on this, a rotor core and magnetic pole structure with protrusion are adopted, while maintaining the same pole arc coefficient and magnet thickness.

Figure 1 Structure of the proposed PMSM and its rotor along with the semi-inset pole pattern (see online version for colours)

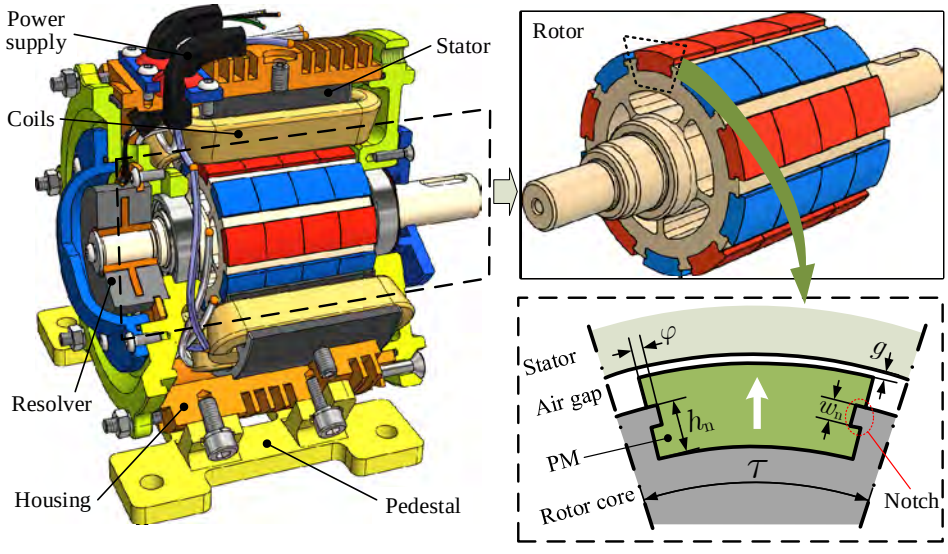

Table 3 The main dimensions of the traditional tile-shaped surface-mounted magnet motor

Item	*Notation*	*Value*	*Unit*
Stator diameter	D_o	86	mm
Stator bore	D_i	51.6	mm
Stator length	l	50	mm
Tooth depth	h	14	mm
Tooth width	w	6	mm
Air gap	δ	0.4	mm
Pole arc coefficient	α	140	deg
Magnet thickness	h_{mag}	4	mm

2.2 Work principle of the proposed pole pattern

As shown in Figure 2, the magnetic circuit at both ends of the magnetic poles has changed in the proposed pole pattern, comparing with the conventional one. Based on the law of equivalent magnetic circuits, the following equation can be derived.

$$H\left(h_{mag}-w_n\right)=B_g l\varphi\left(\frac{(1-\alpha)\tau}{2\mu_0\mu_r h_n l}+\frac{h_{mag}+\delta}{\mu_0\mu_r\varphi l}\right) \tag{1}$$

where h_{mag}, w_n, l, h_n, α, τ and φ are dimensional parameters as shown in Figure 1 and Table 2, B_g is the magnetic flux density in air gap, μ_0 is the vacuum magnetic permeability and μ_r is the relative magnetic permeability.

Figure 2 Structure of the proposed PMSM and its rotor along with its pole pattern (a) magnetic circuit of the conventional rotor (b) magnetic field FEA results of the conventional rotor (c) magnetic circuit of proposed rotor (d) magnetic field FEA results of proposed rotor (see online version for colours)

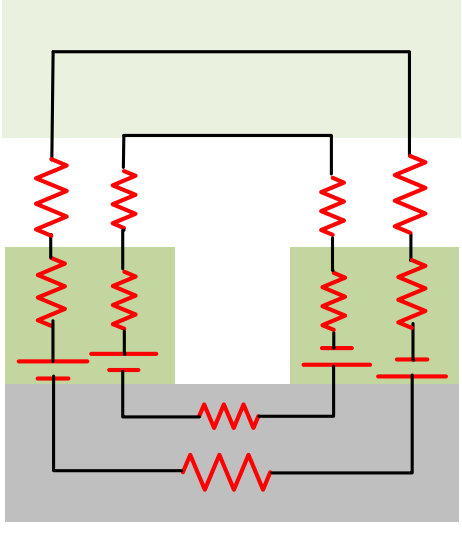

(a)

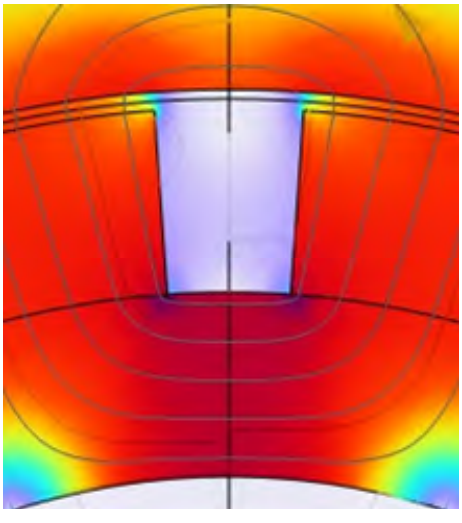

(b)

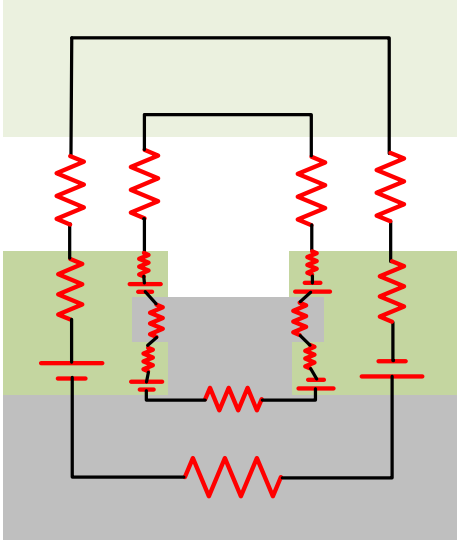

(c)

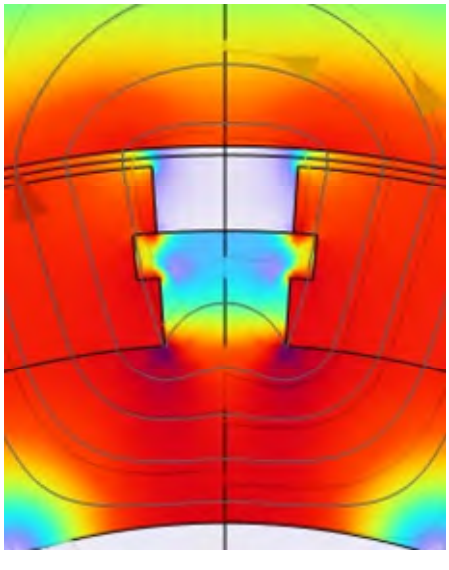

(d)

For the convenience of analysis, the formulas are organised as

$$B_g = \frac{2h_n\mu_0\mu_r H\left(h_{mag} - w_n\right)}{(1-\alpha)\tau\varphi + 2h_n h_{mag} + 2h_n\delta} \tag{2}$$

According to equation (2), it can be seen that the air gap magnetic density at the edge of the magnetic pole is related to the height of the protrusion, the depth and width of the notch. The relationship is obvious. The height of the protrusion can increase the air gap magnetic density to a certain extent, because the magnetic circuit inside the protrusion is widened, resulting in a decrease in this part of the magnetic resistance. The finite element analysis (FEA) results shown in the [Figure 2(b) and 2(d)] also support this. But if the protrusion is too high, there will be no magnetic circuit passing through it, and instead, a part of the magnetic circuit will form a small loop without passing through the air gap, causing a decrease in the air gap. The influence of notches on the air gap may be monotonic, as the width of the notches leads to a decrease in the magnetic electromotive force, and the depth of the notches increases magnetic resistance. Therefore, the influence of notches on the air gap magnetic field is negative.

3 Sensitivity analysis of structural parameters

3.1 Finite element simulation model

In order to further study the influence of structural parameters on electromagnetic performance, a FEA model of electromagnetic field is established. To study the more general laws of structural parameters, the structural parameters are dimensionless and the following three coefficients are defined:

$$\alpha_h = \frac{h_n}{h_{mag}}, \alpha_w = \frac{w_n}{h_n}, \alpha_\varphi = \frac{\varphi}{\alpha\tau} \tag{3}$$

where α_h, α_w, $\alpha_\varphi \in (0, 1)$.

Figure 3 FEA model of the pole pattern for radial air-gap magnetic flux density (see online version for colours)

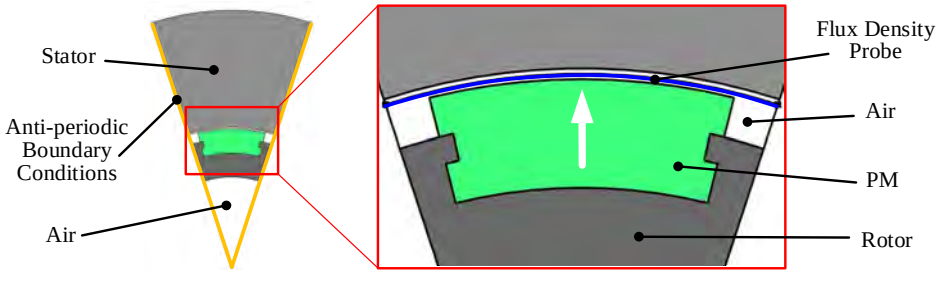

Using a slot-less model to study the air gap magnetic field can eliminate the influence of stator structure on the magnetic field and more easily reveal the influence of magnetic pole configuration on the air gap magnetic density waveform. As shown in Figure 3, an electromagnetic field FEA model of magnetic pole configuration is established by COMSOL 6.2. The magnetisation direction of the permanent magnet is parallel, which is easy to manufacture and has a large air-gap fundamental magnetic flux density. By utilising the symmetry of the structure, the model can be simplified using anti-periodic boundary conditions to improve computational speed. Collect radial magnetic flux

density along an arc in the middle of the air gap, and obtain the radial air gap magnetic flux density waveform. The fundamental magnetic flux density then is obtained by performing Fourier decomposition on the waveform. By parameterising the non-dimensional structural parameters in equation (3), the influence of different structural parameters on the fundamental air gap magnetic density can be obtained.

In theory, the larger the fundamental magnetic density, the greater the output torque of the motor. The effect of stator slot on the fundamental magnetic flux density of the air gap can be directly corrected using the Carter coefficient (Zhu and Howe, 1993). When the stator structure remains unchanged, the torque is proportional to the fundamental magnetic flux density. Therefore, the influence of magnetic pole configuration on the output torque of the slotted motor is consistent with the influence on the fundamental wave of air gap magnetic density in the slot-less model. To validate the improvement on the torque output of the motor, the magnetic pole configuration is imported into motor-CAD for simulation, allowing for the evaluation of the magnetic field distribution and the overall output torque of the motor. Figure 4 presents the mesh and simulation results generated in motor-CAD.

Figure 4 FEA model of the entire motor for torque output (a) regional and element division of the entire rotor (b) FEA results of the entire motor (see online version for colours)

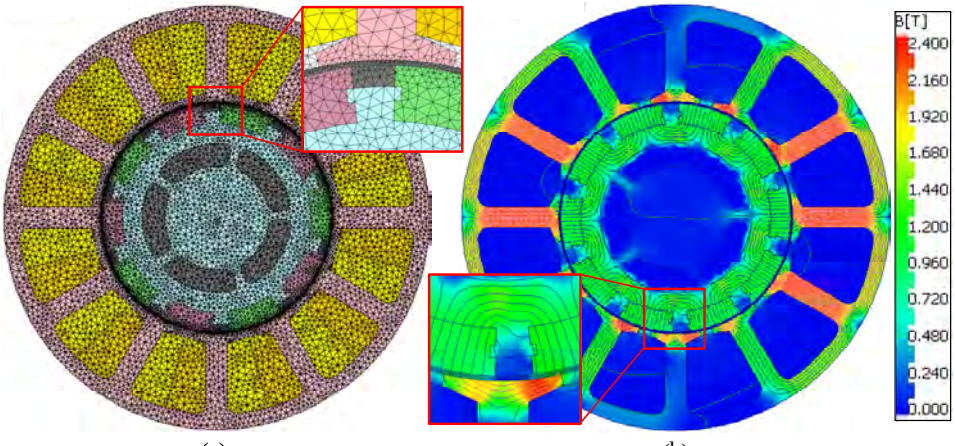

(a) (b)

3.2 Response surface of air gap magnetic density

In order to obtain the influence of structural parameters on the fundamental wave air gap magnetic density, it is assumed that the depth coefficient of the groove is 0.05. Then a parameterised scanning is performed on the protrusion height and notch width coefficients, and the results obtained are shown in Figure 5(a). It is evident that the width of the notch has minimal influence on the fundamental magnetic density, while the height of the protrusion has a greater impact on the fundamental magnetic density of the air gap. The fundamental magnetic density rises initially and decreases as the protrusion height increases subsequently. This is consistent with previous theoretical analysis.

In order to analyse the effect of notch depth on the fundamental wave magnetic density of the air gap, a notch width coefficient of 0.4 is arbitrarily selected, and the

protrusion height and notch depth coefficients are parameterised and swept. The results obtained are shown in Figure 5(b). It is found that the depth of the notch has a significant impact on the fundamental magnetic density of the air gap. As the depth of the notch increases, the fundamental magnetic density of the air gap decreases. Therefore, from an electromagnetic design perspective, the smaller the depth of the notch, the better.

From Figure 5, it can be seen that by selecting appropriate protrusion heights and notch depths, a larger fundamental magnetic flux density can be obtained than the conventional pole pattern. This also means that the proposed pattern can achieve a larger output torque than the original configuration.

Figure 5 Parameter swept results of fundamental magnetic density (a) the fundamental magnetic density varies with protrusion height and notch width (b) the fundamental magnetic density varies with protrusion height and notch depth (see online version for colours)

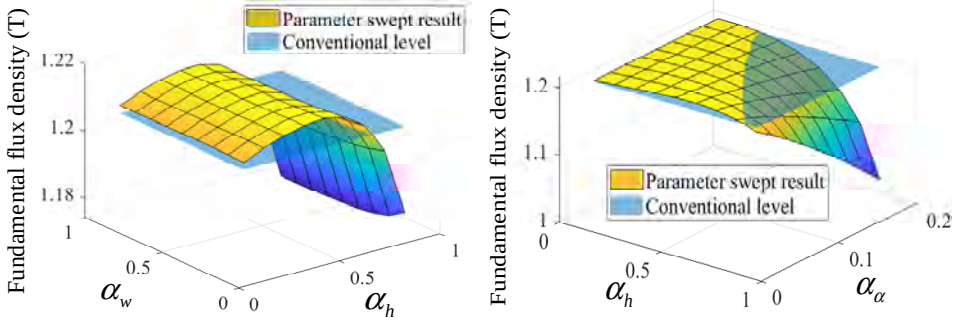

3.3 Validation of torque output

After the above analysis, the final choice is α_h = 0.625, α_h = 0.4, α_φ = 0.05. After inputting the parameters into the FEA model of the motor, as shown in Figure 4, the torque output is obtained. The control method of is simulated.

Figure 6 Comparison between proposed pattern and conventional pattern (a) comparison of torque output (b) comparison of utilisation rate of pm material and torque ripple (see online version for colours)

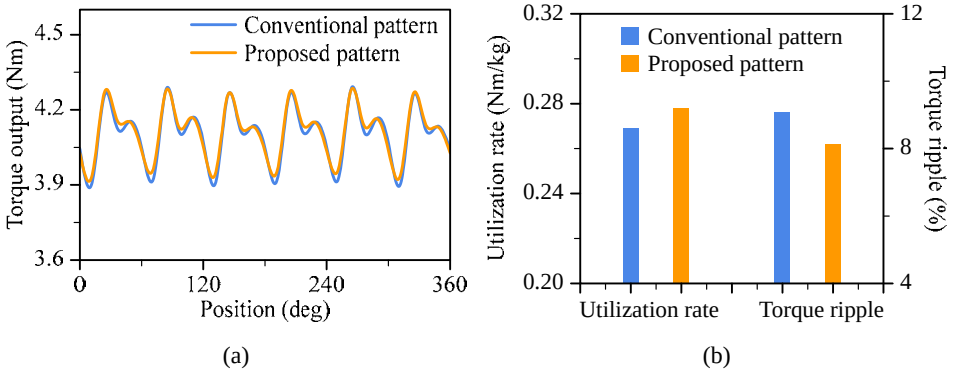

Comparing the output torque of the proposed pole pattern with the conventional one, it can be found that the new pattern can generate greater torque with less PM material usage. Thus, it has high PM utilisation rate, which is the ratio of torque output to PM volume or weight (Boldea et al., 2014; He et al., 2024; Li et al., 2020; Xiang et al., 2024). As shown in the Figure 6, with the same q-axis current of 2.441 A, the average torque output of the proposed motor is 4.1852 Nm, while that of the conventional motor is 4.1588 Nm. Specifically, the torque increase by 0.625% and the usage of magnetic material decreases by 2.50%, which means the PM utilisation rate increase by 3.35%. Furthermore, the torque ripple is also decreased by 10.556%.

4 Simulation of structural strength and temperature rise

4.1 Structural strength verification

In order to verify the structural strength and stiffness of the rotor and ensure its sufficient safety, solid FEA is conducted on the rotor. The rotor's centrifugal force and the electromagnetic attraction exerted by the stator are taken into account. It is also considered that there is a 0.1 mm thick adhesive layer between the PM and the rotor. As shown in Figure 7, the maximum stress of the rotor is concentrated on the spokes on both sides of the weight reduction hole, rather than at the magnetic steel connection position, and it is only 3.57 MPa, far less than the yield limit of the structure. The maximum displacement of the motor is merely 0.216 μm. Therefore, the stiffness is also sufficient, i.e., 0.4 mm thickness of air gap is safe enough.

Figure 7 Structural strength verification results of the rotor (a) strength (b) stiffness (see online version for colours)

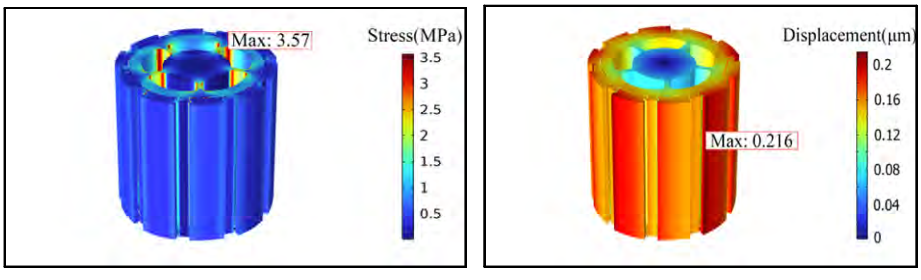

(a) (b)

4.2 Thermal verification

To ensure that the motor can operate normally in the required ambient temperature, temperature simulation is conducted on the motor. A lumped parameter thermal network (LPTN) method is adopted to simulate the temperature of the motor. The LPTN of the motor is established and calculated by Ansys Motor-CAD. The motor is installed horizontally and uses circular fins for natural convection cooling. Taking the loss under rated operating conditions of the motor as the loading condition, the ambient temperature is set to the maximum operating temperature of the motor, which is 70°C. The simulation

results are shown in Figure 8. The highest temperature of the motor winding can reach 137°C, which is lower than the temperature resistance limit of the winding. The maximum temperature of the magnetic steel is 127°C, which is lower than the selected grade of NdFeB magnetic pole, so there is no risk of demagnetisation for the PM.

Figure 8 Thermal verification results of the motor (a) axial view (b) radial view (see online version for colours)

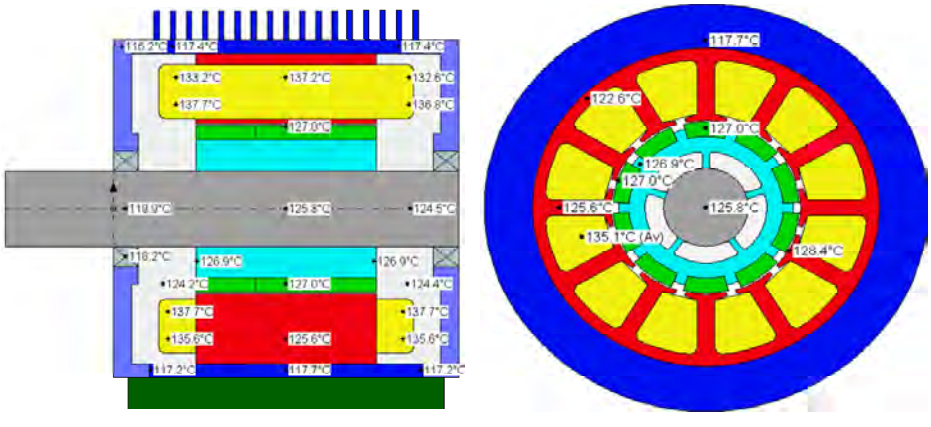

(a) (b)

5 Prototype processing and experimentation

5.1 Prototype processing

As shown in Figure 9, a prototype of the proposed motor is fabricated as shown in Figure 9. The PM is made by wire cut electrical discharge machining (WEDM) and plated by nickel. The outer contour and weight reduction holes of the rotor are also processed by WEDM. Then the PMs are inserted into the slot of the rotor.

Figure 9 Prototypes processing (a) prototype of proposed rotor (b) prototype of the stator and housing (c) prototype of the entire motor (see online version for colours)

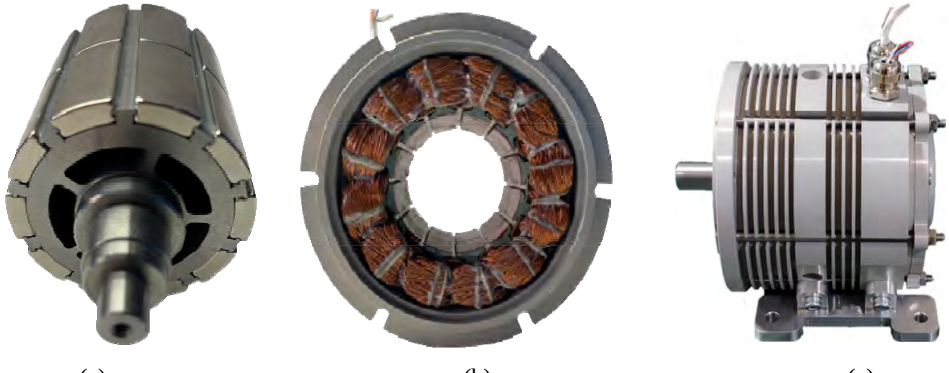

(a) (b) (c)

5.2 Performance testing

In order to test the output performance of the motor, it is installed on a hysteresis dynamometer as shown in Figure 10. The hysteresis dynamometer can provide a braking torque of up to 10 Nm. A torque-speed sensor with a range of 10 Nm and 3,000 r/min is connected to the motor and the dynamometer to read the torque output and shaft speed. The motor is equipped with a thermistor inside, and an ohmmeter measures the resistance of the thermistor to gauge the temperature of the motor winding, avoiding overheating. The motor is driven by a Kollmorgen drive controller, which is commanded by the upper computer to control the motor speed.

Figure 10 Experimental arrangement for the performance test of the prototype (see online version for colours)

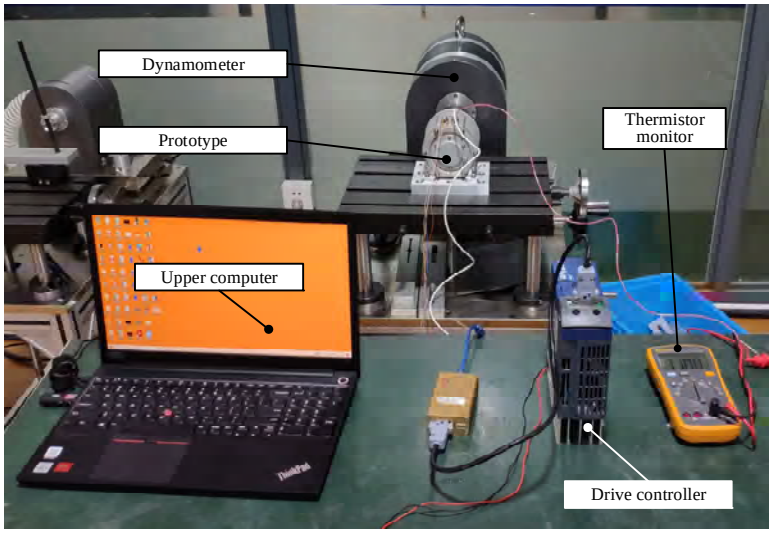

Figure 11 Test results (a) comparison between experimental and simulated results (b) external characteristic and efficiency curve (see online version for colours)

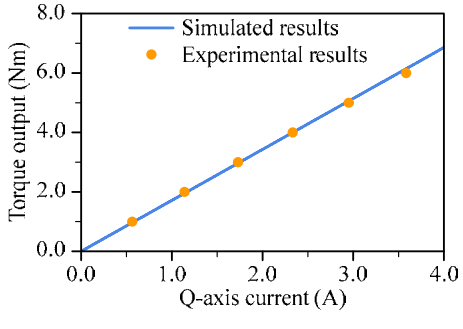

(a)

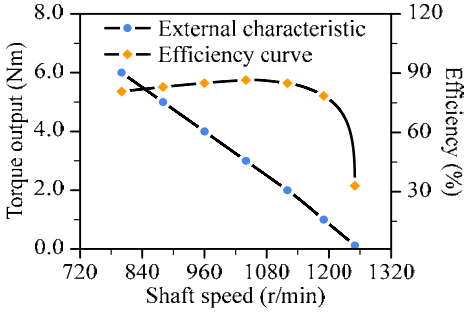

(b)

Firstly, the difference between the output torque of the motor and the simulation results is verified. After rotating the motor to 800 r/min, the load on the dynamometer is increased, and the driving current under different loading torques is tested. Figure 11(a) displays the results, which are largely in agreement with the simulation findings. As the load increases, the torque coefficient obtained from the experiment decreases. This is caused by the saturation of the stator along with the temperature rising on the PM and stator laminations. Secondly，the motor's external characteristic curve and efficiency curve are tested. As shown in Figure 11(b), the designed motor can meet the design indicators in Table 1.

6 Conclusions

In this paper, a torque motor with enhanced performance employing novel semi-inset PM pole is proposed. The rotor has a protrusion that insert between PMs and the PMs also has notch so that the rotor and PMs are embedded together. This design has the potential to boost the motor's output performance and strengthen the rotor's structure. The major works are concluded as follows:

1 The design requirements and overall structure are introduced. The work principle of the proposed pole pattern is illustrated. Through analytical analysis, the superiority of the proposed configuration and the impact of structural parameters on performance are demonstrated

2 A FEA model of the motor and magnetic pole is established, and a detailed analysis of how structural parameters affect electromagnetic performance is conducted. Through comparison, it is found that selecting appropriate structural parameters can indeed achieve better output performance than conventional magnetic pole configurations. Afterwards, the structural strength and temperature rise of the motor are verified, and there is no risk of detachment or demagnetisation of the magnetic steel.

3 One research prototype of the electric motor with the optimised structure has been developed, and experiments are conducted on the torque output and the external characteristic. The experimental results are compared with the numerical simulation, and the comparison shows the consistency between. Thus, the proposed design is validated.

Acknowledgements

This research was funded in part by the National Key R&D Program of China under Grant 2022YFE0113700, in part by the National Natural Science Foundation of China under Grant 52130505, in part by the Zhejiang Provincial Natural Science Foundation of China under Grant LD24E050005, in part by the Ningbo Key Scientific and Technological project under Grant 2022Z040, in part by the Aeronautical Science Foundation of China under Grant 20200007051002, and in part by the Fundamental Research Funds for the Central Universities.

Declarations

All authors declare that they have no conflicts of interest.

References

Ashabani, M. and Mohamed, Y.A-R.I. (2011) 'Multiobjective shape optimization of segmented pole permanent-magnet synchronous machines with improved torque characteristics', *IEEE Trans. Magn.*, Vol. 47, No. 4, pp.795–804.

Boldea, I., Tutelea, L.N., Parsa, L. and Dorrell, D. (2014) 'Automotive electric propulsion systems with reduced or no permanent magnets: an overview', *IEEE Trans. Ind. Electron.*, Vol. 61, No. 10, pp.5696–5711.

Burress, T.A., Campbell, S.L., Coomer, C., Ayers, C.W., Wereszczak, A.A., Cunningham, J.P., Marlino, L.D., Seiber, L.E. and Lin, H-T. (2011) *Evaluation of the 2010 Toyota Prius Hybrid Synergy Drive System* (No. ORNL/TM-2010/253), Oak Ridge National Lab. (ORNL), Oak Ridge, TN (United States), Power Electronics and Electric Machinery Research Facility.

Ding, H., Li, Y., Zhu, Q. and Su, J. (2024) 'Position servo with variable speed pump-controlled cylinder: design, modelling and experimental investigation', *International Journal of Hydromechatronics*, Vol. 7, No. 2, pp.155–175.

Dong, Z., Yan, L., Su, H. and Chen, I-M. (2024) 'Design and analysis of a novel electromagnetic-propulsion rotary machine with external blending-shaped tessellation magnet pattern', *IEEE Trans. Ind. Electron.*, Vol. 71, No. 2, pp.1355–1364.

Hall, D., Chin, J., Anderson, A., Smith, A., Edwards, R. and Duffy, K.P. (2019) 'Development of a Maxwell X-57 high lift motor reference design', *AIAA Propulsion and Energy 2019 Forum, American Institute of Aeronautics and Astronautics*, Indianapolis, IN.

He, X., Yan, L., Xiang, P., Du, N., Liu, X. and Liu, J. (2023) 'Multi-objective optimization method for surface-mounted PMSM with fixed torque output', *2023 26th International Conference on Electrical Machines and Systems* (*ICEMS*), pp.4904–4908.

He, X., Yan, L., Xiang, P., Du, N., Liu, X., Chen, I-M. and Hu, H. (2024) 'Multimaterial topology optimization method of surface-mounted pmsm rotor poles based on variable density representation', *IEEE/ASME Trans. Mechatron.*, pp.1–11, Early access.

Hsu, J.S. (2004) *Report on Toyota/Prius Motor Design and Manufacturing Assessment* (No. ORNL/TM-2004/137), Oak Ridge National Lab. (ORNL), Oak Ridge, TN (United States).

Isfahani, A.H., Vaez-Zadeh, S. and Rahman, M.A. (2008) 'Using modular poles for shape optimization of flux density distribution in permanent-magnet machines', *IEEE Trans. Magn.*, Vol. 44, No. 8, pp.2009–2015.

Jang, S-M., Park, H-I., Choi, J-Y., Ko, K-J. and Lee, S-H. (2011) 'Magnet pole shape design of permanent magnet machine for minimization of torque ripple based on electromagnetic field theory', *IEEE Trans. Magn.*, Vol. 47, No. 10, pp.3586–3589.

Li, J., Wang, K. and Zhang, H. (2020) 'Flux-focusing permanent magnet machines with modular consequent-pole rotor', *IEEE Trans. Ind. Electron.*, Vol. 67, No. 5, pp.3374–3385.

Liu, X., Chen, H., Zhao, J. and Belahcen, A. (2016) 'Research on the performances and parameters of interior PMSM used for electric vehicles', *IEEE Trans. Ind. Electron.*, Vol. 63, No. 6, pp.3533–3545.

Liu, Y., Zhu, Z.Q. and Howe, D. (2007) 'Commutation-torque-ripple minimization in direct-torque-controlled PM brushless DC drives', *IEEE Trans. Ind. Appl.*, Vol. 43, No. 4, pp.1012–1021.

Lu, X., Iyer, K.L.V., Mukherjee, K., Ramkumar, K. and Kar, N.C. (2015) 'Investigation of permanent-magnet motor drives incorporating damper bars for electrified vehicles', *IEEE Trans. Ind. Electron.*, Vol. 62, No. 5, pp.3234–3244.

Panwar, P. and Michael, P. (2018) 'Empirical modelling of hydraulic pumps and motors based upon the Latin hypercube sampling method', *International Journal of Hydromechatronics*, Vol. 1, No. 3, pp.272–292.

Pyrhonen, J., Jokinen, T. and Hrabovcova, V. (2013) *Design of Rotating Electrical Machines*, John Wiley & Sons, UK.

Qiu, Z., Chen, Y., Liu, X., Zhang, L. and Cheng, H. (2022) 'Evaluation and comparison of sideband harmonics and acoustic responses with continuous and discontinuous PWM strategies in permanent magnet synchronous motor for electric vehicles', *International Journal of Hydromechatronics*, Vol. 5, No. 2, pp.109–123.

Shen, Y., Zhu, Z.Q. (2012) 'Investigation of permanent magnet brushless machines having unequal-magnet height pole', *IEEE Trans. Magn.*, Vol. 48, No. 12, pp.4815–4830.

Xiang, P., Yan, L., Guo, Y., He, X., Gerada, C. and Chen, I-M. (2024) 'A concentrated-flux-type PM machine with irregular magnets and iron poles', *IEEE/ASME Trans. Mechatron.*, Vol. 29, No. 1, pp.691–702.

Xiang, P., Yan, L., Xiao, H., He, X. and Du, N. (2023) 'Development of a novel radial-flux machine with enhanced torque profile employing quasi-cylindrical PM pattern', *IEEE Trans. Energy Convers.*, Vol. 38, No. 4, pp.2772–2783.

Yamazaki, K., Utsunomiya, K., Tanaka, A. and Nakada, T. (2022) 'Rotor surface optimization of interior permanent magnet synchronous motors to reduce both rotor core loss and torque ripples', *IEEE Trans. Ind. Appl.*, Vol. 58, No. 4, pp.4488–4497.

Yan, L., Chen, I-M., Lim, C.K., Yang, G., Lin, W. and Lee, K-M. (2008) 'Design and analysis of a permanent magnet spherical actuator', *IEEE/ASME Trans. Mechatron.*, Vol. 13, No. 2, pp.239–248.

Yan, L., Chen, I-M., Yang, G. and Lee, K-M. (2006) 'Analytical and experimental investigation on the magnetic field and torque of a permanent magnet spherical actuator', *IEEE/ASME Trans. Mechatron.*, Vol. 11, No. 4, pp.409–419.

Yan, L., Liu, Y., Zhang, L., Jiao, Z. and Gerada, C. (2019) 'Magnetic field modeling and analysis of spherical actuator with two-dimensional longitudinal camber halbach array', *IEEE Trans. Ind. Electron.*, Vol. 66, No. 12, pp.9112–9121.

Yu, Y., Pei, Y. and Chai, F. (2023) 'Power factor analysis in spoke-type permanent magnet vernier motors with different slot–pole combinations for in-wheel direct drive', *IEEE Transactions on Transportation Electrification*, Vol. 9, No. 1, pp.642–655.

Zeng, Y., Cheng, M., Liu, G. and Zhao, W. (2020) 'effects of magnet shape on torque capability of surface-mounted permanent magnet machine for servo applications', *IEEE Trans. Ind. Electron.*, Vol. 67, No. 4, pp.2977–2990.

Zhang, Y., Gono, R. and Jasiński, M. (2023) 'An improvement in dynamic behavior of single phase PM brushless DC motor using deep neural network and mixture of experts', *IEEE Access*, Vol. 11, pp.64260–64271.

Zheng, P., Zhao, J., Han, J., Wang, J., Yao, Z. and Liu, R. (2007) 'Optimization of the magnetic pole shape of a permanent-magnet synchronous motor', *IEEE Trans. Magn.*, Vol. 43, No. 6, pp.2531–2533.

Zhu, Z.Q. and Howe, D. (1993) 'Instantaneous magnetic field distribution in brushless permanent magnet DC motors. III. Effect of stator slotting', *IEEE Trans. Magn.*, Vol. 29, No. 1, pp.143–151.